Letter

Coherent multistep rovibrational excitation using intense midinfrared pulses

Hiroki Tsusaka, Ikki Morichika, and Satoshi Ashihara
Institute of Industrial Science, The University of Tokyo, 4-6-1 Komaba, Meguro-ku, Tokyo 153-8505, Japan

(Received 31 May 2024; accepted 20 November 2024; published 9 December 2024)

We experimentally demonstrate coherent multistep rovibrational excitation in gas-phase carbon dioxide using intense midinfrared laser pulses. Ultrafast pump-probe spectroscopy directly observes excited-state rovibrational lines up to $V = 11$ state with rotational quantum numbers of $J = 0 - 40$. The observed signal for each transition line is found to oscillate with the pump-probe delay time, attributed to rotational beats based on higher-order nonlinear response function theory. These results indicate generation of rotational wave packets in the high-lying vibrational states, which paves the way toward mode-selective stereochemistry at the electronic ground-state.

DOI: 10.1103/PhysRevResearch.6.L042058

Introduction. Controlling molecular processes with coherent laser sources remains a topic of great interest [1–7]. In contrast to traditional thermodynamic methods that depend on temperature and pressure, the direct control of quantum states through coherent light-matter interactions offers a means to drive chemical reactions with enhanced efficiency and selectivity. One effective knob of coherent control is the vibrational degree of freedom. Chemical reactions can be directed along a specific pathway by exciting the key reagent vibration in reactant molecules through electronic, infrared, or Raman processes [8]. Another promising knob is the rotational degree of freedom. The mutual orientation of interacting molecules has a great impact on bimolecular reactions and gas-surface reactions, known as stereodynamic effects [9,10]. Various schemes for aligning or orienting molecules have been demonstrated, such as adiabatic nonresonant laser interaction [11,12], nonadiabatic (impulsive Raman) excitation [13], optical centrifuges [14], and resonant THz excitation [15,16].

Infrared radiation offers a distinctive way to excite both vibrational and rotational motions of molecules while remaining in the electronic ground state. Since direct excitation to highly-excited rovibrational states is inefficient due to the small transition dipole moment, step-wise excitation that passes through a series of intermediate states is a more promising route. Although this approach has faced the detuning caused by molecular anharmonicity; the transition frequencies decrease while climbing the ladder, recent advancements in infrared ultrafast lasers that cover the multiple transitions have opened up the way to efficient vibrational ladder climbing (VLC). The VLC has been applied to a variety of molecules, including metal carbonyls [17,18], NO [19], CH_2H_2 [20], Hb − CO [21], and amino acids [22], and has been shown to trigger ground-state dissociation of small molecules in the gas phase [17,18,20]. Down chirping has proved useful in achieving efficient VLC by maintaining resonance with the subsequent steps [23], and arbitrary pulse shaping has been exploited for selective population of the excited vibrational states [24]. Furthermore, in combination with plasmonic field enhancement, ground-state dissociation of $W(CO)_6$ in the condensed phase has been recently demonstrated [25].

Despite the intensive studies, however, most of them have only focused on vibrational excitation. In the condensed phase, rotational states can be ignored due to quenched rotational motion. However, in the gas phase, the rotational motion is well quantized and rotational excitation inevitably occurs together with vibrational excitation. Therefore, there is still much to be explored in terms of implementing rotational excitation in addition to vibrational excitation simultaneously for achieving even greater control over molecular reactions. In this Letter, we report on experimental demonstration of coherent multistep rovibrational excitation in the antisymmetric stretching mode (ν_3) of gas-phase carbon dioxide (CO_2) via intense midinfrared pulses (Fig. 1). By use of spectrally resolved pump-probe spectroscopy, we prove generation of rotational wave packets (RWPs) at vibrationally excited states of $V = 0 - 11$.

Experimental method. We prepare a homemade gas cell with the optical path length of 1 mm, same as the spatial

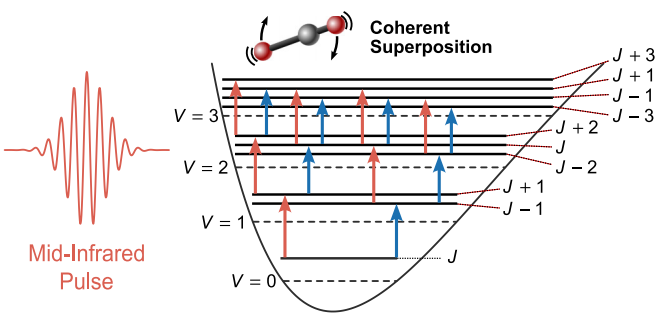

FIG. 1. Schematic of coherent multistep rovibrational excitation with midinfrared laser pulses.

overlap length between the pump and probe pulses (see Sec. I in the Supplemental Material [26]). The gas cell is filled with gaseous CO_2 molecules at a pressure of 0.3 atm. Figure 2(a) shows the absorption spectrum of the sample measured with an FTIR spectrometer. The observed absorption lines are attributed to the rovibrational transitions of the ν_3 mode. There are two separated branches centered at 2350 cm^{-1} following the selection rules: $\Delta J = -1$ (P branch) and $\Delta J = +1$ (R branch), where J is the total angular momentum quantum number. Each absorption line stems from a transition of different initial rotational levels that are thermally populated. Due to the symmetry of $D_{\infty h}$, only even (odd) rotational levels are allowed at each even (odd) vibrational level in CO_2, and the pure vibrational transition of $\Delta J = 0$ (Q branch) is formally forbidden.

We perform spectrally resolved infrared pump-probe spectroscopy for probing multistep rovibrational excitation in the ν_3 mode with the following system. An amplified Ti:sapphire laser (Solstice Ace, Spectra Physics) that generates 90 fs, 7 mJ, 800 nm pulses at a 1 kHz repetition rate is used to pump an optical parametric amplifier followed by difference frequency generation (TOPAS, Light Conversion). The generated midinfrared pulses are 100 μJ in energy and centered at 2250 cm^{-1} with a fwhm bandwidth of 180 cm^{-1}. The midinfrared pulse is split into pump and probe pulses, focused and spatially overlapped in the sample, where the fluence of the pump pulse is 32 mJ cm^{-2}. The transmitted probe pulses are dispersed by a 320 mm monochromator (iHR320, Horiba) with a 300 line mm^{-1} grating and detected on a thermoelectrically cooled, 256 pixel PbSe detector array (B-LC5T-256R, Infrared Materials). This system is capable of spectral measurement with a high resolution of 0.5 cm^{-1} over a wide span of 128 cm^{-1}. The setup is continuously purged with dry nitrogen to suppress atmospheric background signals.

Results. Figure 2(b) shows the measured transient spectra in terms of the absorbance change as a function of the pump-probe delay time. Absorbance changes are clearly observed across a wide frequency range beyond the linear absorption band. Considering the vibrational anharmonic shift of 25 cm^{-1} [27], the frequency range reaches up to the $V = 10 \rightarrow 11$ transition frequency. The complexity of the observed spectrum comes from the spectral overlap of the rovibrational lines of different vibrational states. Indeed, the anharmonic shift is smaller than the frequency distribution of the rovibrational transitions from the same initial vibrational states. Since the distribution of the J numbers broadens with the cascading transitions, identification of each transition line is more challenging for higher vibrational states. For example, the frequency deviation between $|V, J\rangle = |2, 2\rangle \rightarrow |3, 1\rangle$ and $|3, 35\rangle \rightarrow |4, 34\rangle$ transitions is theoretically predicted to be 0.0015 cm^{-1}, which is difficult to resolve with our spectral resolution.

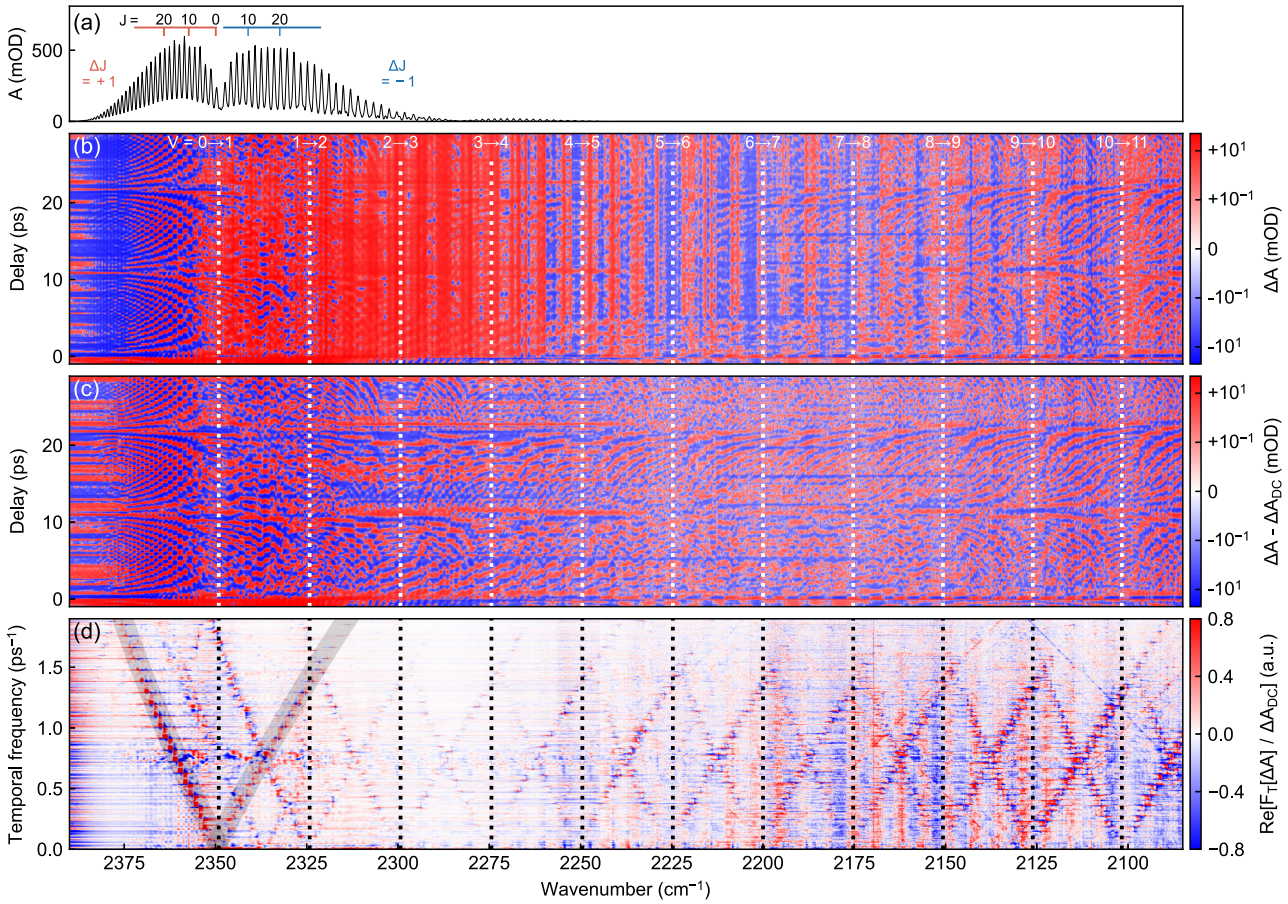

FIG. 2. (a) The measured absorption spectrum of the sample. (b) Transient absorbance change spectra at varied delay times. (c) Transient absorbance change spectra subtracted with the DC component and (d) their real part of the Fourier transform in terms of the delay time.

In addition to the long-lasting components due to the excited population states, there can be clearly seen the oscillations of the signals for each rovibrational line with the delay time. Notably, this behavior is characteristic of the gas phase, which is not observed in the condensed phase [28]. To better visualize the oscillatory structures, we remove the DC component from the observed signals, as shown in Fig. 2(c). Although the oscillation frequencies are different for each rovibrational line, there can be seen a periodic structure at a period of approximately 11 ps. Note that this feature is well reproduced by the numerical simulation based on the Liouville von Neumann equation (see Sec. II in the Supplemental Material [26]).

Discussion. To gain insight into the origin of the oscillations, we perform Fourier transform along with the delay time ranging from 0 ps to 300 ps. Figure 2(d) shows the obtained two-dimensional spectrum. Here we display the real part of the Fourier spectrum, normalized by its DC component at each optical frequency. There can be seen the multiple V-shape structures centered at $|V, J = 0\rangle \rightarrow |V + 1, J = 0\rangle$ frequencies, which means that the oscillation frequency linearly scales with the J numbers for each vibrational state. The similar oscillation has been experimentally observed in two-dimensional infrared (2D-IR) spectroscopy for gaseous CO_2 molecules [29], and theoretically investigated based on third-order response function theory [30]. Below, we will analyze the physical origin of the oscillation by extending the previously reported theory into higher order.

We consider the case that the pump and probe pulses with the semi-impulsive envelopes interact with the molecules. The emitted field in the probe beam direction is represented by

$$E_{\mathrm{sig}}(t, T) \propto i \sum_n P^{(2n+1)}(t, T) = i \sum_n \mathcal{E}_{\mathrm{pu}}^{2n} \mathcal{E}_{\mathrm{pr}} \sum_m R_m^{(2n+1)}(t, T), \quad (1)$$

where $P^{(2n+1)}$ is the nonlinear polarization (n: integer), t is the time interval between the probe interaction and the signal detection, T is the pump-probe delay time, $R_m^{(2n+1)}$ is the nonlinear response function for each Liouville pathway indexed by integer m, and $\mathcal{E}_{\mathrm{pu}}$, $\mathcal{E}_{\mathrm{pr}}$ are the pulse areas of the pump and probe pulses, respectively. Considering the phase matching condition, the signal consists of radiation from $(2n + 1)$th order polarization, generated by the $(2n)$th pump interactions and the linear probe interaction. Here we assume that the probe interaction is linear due to the weak interaction energy of 3.6×10^{-22} J (pulse area of 0.11π).

Focusing on the part corresponding to the probe interaction and the following signal emission, there are eight possible Liouville pathways based on the phase matching condition and the selection rule of $\Delta J = \pm 1$ and $\Delta V = \pm 1$, as shown in Fig. 3. Here we use a compact notation, inspired by the shorthand method introduced by Mandal *et al* [31]: the *final* rovibrational state is labeled by $|V, J\rangle \equiv |0\rangle$, and the *followed* states are identified by the difference in their quantum number, that is, $|V + 1, J + 1\rangle \equiv |1R\rangle$, $|V + 1, J - 1\rangle \equiv |1P\rangle$, $|V, J + 2\rangle \equiv |0S\rangle$, and $|V, J - 2\rangle \equiv |0O\rangle$, where the rotational letters follow standard spectroscopic notation. The diagrams are categorized based on the transition type of the emission process (left half: R branch, right half: P branch) and the state during the delay time (top half: population state, bottom half: coherence state). For each category, there are two types of signal emission processes: excited-state absorption (ESA) and stimulated emission (SE). It should be noted that the rotationally coherent (RC) pathways are unique to gas-phase molecules, in which vibrational transitions are accompanied by rotational transitions.

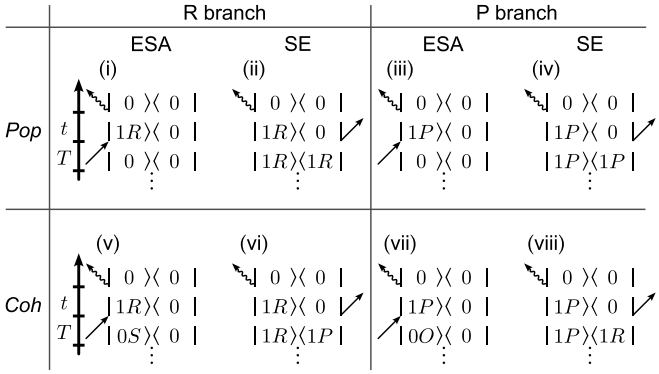

FIG. 3. All possible double sided Feynmann diagrams which start from the state after multiple interactions of the pump pulse. The pathways in the upper row pass through the population state, while those in the lower row pass through the coherence state.

The nonlinear response functions for the population and RC pathways are given by

$$R_{m,\mathrm{pop}}^{(2n+1)}(t, T) = \frac{i(-1)^{n+\lambda}}{\hbar^{2n+1}} [\Pi_i \mu_i] \times \exp[-\gamma_{\mathrm{pop}} T] \exp[-(i\omega_{\mathrm{rad}} + \gamma_{\mathrm{rad}})t], \quad (2)$$

$$R_{m,\mathrm{coh}}^{(2n+1)}(t, T) = \frac{i(-1)^{n+\lambda}}{\hbar^{2n+1}} [\Pi_i \mu_i] \times \exp[-(i\Omega_{\mathrm{coh}} + \gamma_{\mathrm{coh}})T] \times \exp[-(i\omega_{\mathrm{rad}} + \gamma_{\mathrm{rad}})t], \quad (3)$$

respectively. Here λ is the number of bra-side interactions in the pathway and $\Pi_i \mu_i$ is the product of the transition moment of ith interaction. The rest terms contain purely the time dependence of the response, where ω_{rad}, Ω_{coh} are the optical frequency of the emitted field and the frequency of the coherence state, respectively, and we include phenomenological relaxation constants: the population relaxation γ_{pop}, the coherence relaxation γ_{coh}, and the dephasing of the radiation γ_{rad}. The response function for the population pathway contains only decay terms, whereas that for the RC pathway includes oscillatory terms with respect to the delay time. These correspond to the DC and AC components observed in the absorption change spectra, respectively.

The oscillation frequencies for the RC pathways are given by the energy difference between ket and bra sides of the density matrix:

$$\Omega_{|0S\rangle\langle 0|} = B_V(4J + 6) \quad : \text{ESA in R branches}, \quad (4)$$

$$\Omega_{|1R\rangle\langle 1P|} = B_{V+1}(4J + 2) \quad : \text{SE in R branches}, \quad (5)$$

$$\Omega_{|0O\rangle\langle 0|} = -B_V(4J - 2) \quad : \text{ESA in P branches}, \quad (6)$$

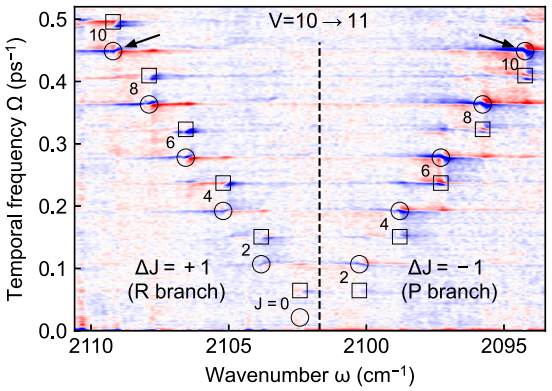

FIG. 4. An enlarged view of Fig. 2(d) around the $V = 10 \rightarrow 11$ transition frequency. The circle (square) markers indicate the signals from stimulated emission (excited state absorption).

$$\Omega_{|1P\rangle\langle 1R|} = -B_{V+1}(4J + 2) \quad : \text{SE in P branches}, \tag{7}$$

where B_V is the rotational constant for the Vth vibrational level. Figure 4 displays the enlarged view of Fig. 2(d) around the $V = 10 \rightarrow 11$ transition frequency, along with the points of $(\omega_{\text{rad}}, \Omega_{\text{coh}})$ calculated using Eqs. (4)–(7) with the previously reported parameters [27]. The calculated points agree well with each peak position in the V-shape structure. By using Eqs. (4)–(7), we perform a global fit to the observed oscillation frequencies, and obtain the V-dependent rotational constants, which are in good agreement with values measured by linear near-infrared spectroscopy in the previous studies (see Sec. III in the Supplemental Material [26]).

The periodic structure observed in the absorbance change spectra [see Fig. 2(c)] can be explained by the derived beat frequencies. In our experiments, the time duration of the pump pulse (150 fs) is sufficiently shorter than the rotational period (∼10 ps) so that the initial phases of the induced rotational coherence can all be regarded as the same. Since the beat frequencies described as Eqs. (4)–(7) approach $4BJ$ for large J numbers, the induced rotational coherence will be in phase at a period of $1/4B$. Furthermore, due to inversion symmetry of CO_2 molecules, the signal can be in phase at half the period ($1/8B$). The estimated recurrence period of 10.7 ps well matches with the observed period, providing direct evidence of the generation of RWPs at each of the excited vibrational states.

The preceding discussion has successfully explained the oscillation frequencies with respect to the delay time observed in the absorbance change spectra. In the rest of this Letter, let us discuss on the spectral line shape for each rotational beat in the two-dimensional spectrum. Figure 5 shows a closer look at the signals corresponding to the stimulated emission from $|11, 11\rangle \rightarrow |10, 10\rangle$ (R branch) and $|11, 9\rangle \rightarrow |10, 10\rangle$ (P branch) transitions. There can be seen a dispersive line shape in both vertical and horizontal directions. Moreover, the line shape is found to be reversed between the R and P branches.

By performing two-dimensional Fourier transform of the response function [Eq. (3)] in terms of t and T, we obtain the spectral line shape of the two-dimensional spectrum expressed

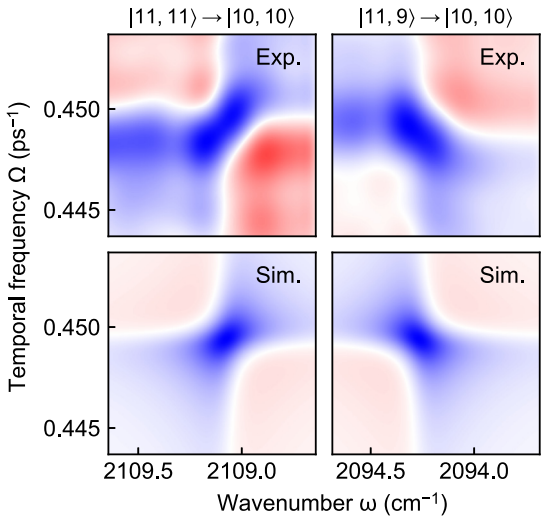

FIG. 5. A closer look at the two-dimensional spectrum corresponding to the stimulated emission from $|11, 11\rangle \rightarrow |10, 10\rangle$ (R branch) and $|11, 9\rangle \rightarrow |10, 10\rangle$ (P branch) transitions as marked with arrows in Fig. 4. The upper (lower) row shows the experimental (simulated) data.

as

$$\Delta A(\omega, \Omega) \propto (-1)^{n+\lambda}(A(\omega - \omega_{\text{rad}}, \gamma_{\text{rad}})A(\Omega - \Omega_{\text{coh}}, \gamma_{\text{coh}}) \pm D(\omega - \omega_{\text{rad}}, \gamma_{\text{rad}})D(\Omega - \Omega_{\text{coh}}, \gamma_{\text{coh}})), \tag{8}$$

where we define $A(\omega, \gamma) \equiv \gamma/(\omega^2 + \gamma^2)$ and $D(\omega, \gamma) \equiv \omega/(\omega^2 + \gamma^2)$ as real and imaginary parts of the complex-valued Lorentzian function, respectively (see Sec. IV in the Supplemental Material [26] for a detailed description). The upper (lower) sign is associated with the emission from the P (R) branches. As shown in Fig. 5, the spectral line shapes calculated from Eq. (8) reproduce the experimental data well. This agreement confirms the coherent nature of the demonstrated multistep rovibrational excitation process. It is noted that the spectral line shapes shown in Fig. 5 are similar to the ones observed in 2D-IR spectroscopy (see Sec. IV in the Supplemental Material [26] for a detailed description).

Conclusion. We successfully demonstrate coherent multistep rovibrational excitation in the ν_3 mode of gaseous CO_2 via intense midinfrared laser pulses. Spectrally resolved pump-probe spectroscopy directly observes absorption changes for rovibrational transitions up to the $V = 11$ state with the rotational quantum numbers of $J = 0 - 40$, as well as those oscillations with respect to the delay time. Based on the higher-order nonlinear response function theory, the oscillation frequencies are attributed to the rotational beats, and the spectral line shape of the two-dimensional spectrum for the RC pathways are explained in a manner similar to 2D-IR spectroscopy. The excellent agreement between the experimental results and theoretical analyses prove the coherent multistep rovibrational excitation up to $V = 11$ and the generation of the RWPs at each of the excited vibrational states.

This unprecedented coherent rovibrational excitation indicates the possibility of high-resolution higher-order multidi-

mensional spectroscopy [32]. Notably, the vibrational energy of the $V = 11$ state is approximately 3.0 eV, corresponding to 55% of the bond dissociation energy (5.45 eV) of CO_2 molecules [33], and beyond typical activation barriers for metal-catalyzed CO_2 conversions (<1.0 eV) [34]. This indicates the promising ability of the midinfrared excitation to control the conversion process. The use of higher power, broadband infrared lasers as well as temporal waveform shaping would improve excitation efficiency. Manipulation of the waveform and polarization of the excitation pulses can allow for more sophisticated control of the multistep rovibrational excitation process. For example, by applying such shaped pulses to a molecular beam or cold molecules trapped in an optical lattice, it should be possible to achieve ladder climbing for both vibration and rotation and coherent population transfer to a certain rovibrational level. Together with the further development of midinfrared laser technologies and optimal control theories, this study paves the way toward mode-selective stereochemistry at the electronic ground state [35,36] and quantum information processing in a cold molecular system [37].

Acknowledgements. The authors thank H. Ueta (Advanced Science Research Center, Japan Atomic Energy Agency) and K. Fukutani (Institute of Industrial Science, The University of Tokyo) for their technical support and valuable discussion. This work was supported by JSPS KAKENHI Grants No. 20K20556, No. 20K22518, and No. 21K14584, and by JST CREST Grant No. JP20348765.

[1] Y. Ohtsuki, M. Sugawara, H. Kono, and Y. Fujimura, Quantum control of molecular reaction dynamics by laser pulses: Development of theory and its application, Bull. Chem. Soc. Jpn. **74**, 1167 (2001).

[2] K. Ohmori, Wave-packet and coherent control dynamics, Annu. Rev. Phys. Chem. **60**, 487 (2009).

[3] C. Brif, R. Chakrabarti, and H. Rabitz, Control of quantum phenomena: past, present and future, New J. Phys. **12**, 075008 (2010).

[4] D. Keefer and R. de Vivie-Riedle, Pathways to new applications for quantum control, Acc. Chem. Res. **51**, 2279 (2018).

[5] K. Heyne and O. Kühn, Infrared laser excitation controlled reaction acceleration in the electronic ground state, J. Am. Chem. Soc. **141**, 11730 (2019).

[6] C. P. Koch, M. Lemeshko, and D. Sugny, Quantum control of molecular rotation, Rev. Mod. Phys. **91**, 035005 (2019).

[7] Q.-Q. Hong, Z.-Z. Lian, C.-C. Shu, and N. E. Henriksen, Quantum control of field-free molecular orientation, Phys. Chem. Chem. Phys. **25**, 32763 (2023).

[8] F. F. Crim, Vibrational state control of bimolecular reactions: Discovering and directing the chemistry, Acc. Chem. Res. **32**, 877 (1999).

[9] A. J. Orr-Ewing, Dynamical stereochemistry of bimolecular reactions, J. Chem. Soc., Faraday Trans. **92**, 881 (1996).

[10] R. N. Zare, Laser control of chemical reactions, Science **279**, 1875 (1998).

[11] H. Sakai, C. P. Safvan, J. J. Larsen, K. M. Hilligsoe, K. Hald, and H. Stapelfeldt, Controlling the alignment of neutral molecules by a strong laser field, J. Chem. Phys. **110**, 10235 (1999).

[12] H. Sakai, S. Minemoto, H. Nanjo, H. Tanji, and T. Suzuki, Controlling the orientation of polar molecules with combined electrostatic and pulsed, nonresonant laser fields, Phys. Rev. Lett. **90**, 083001 (2003).

[13] F. Rosca-Pruna and M. J. J. Vrakking, Experimental observation of revival structures in picosecond laser-induced alignment of I_2, Phys. Rev. Lett. **87**, 153902 (2001).

[14] D. M. Villeneuve, S. A. Aseyev, P. Dietrich, M. Spanner, M. Y. Ivanov, and P. B. Corkum, Forced molecular rotation in an optical centrifuge, Phys. Rev. Lett. **85**, 542 (2000).

[15] H. Harde, S. Keiding, and D. Grischkowsky, THz commensurate echoes: Periodic rephasing of molecular transitions in free-induction decay, Phys. Rev. Lett. **66**, 1834 (1991).

[16] S. Fleischer, Y. Zhou, R. W. Field, and K. A. Nelson, Molecular orientation and alignment by intense single-cycle THz pulses, Phys. Rev. Lett. **107**, 163603 (2011).

[17] L. Windhorn, T. Witte, J. S. Yeston, D. Proch, M. Motzkus, K. L. Kompa, and W. Fuß, Molecular dissociation by mid-IR femtosecond pulses, Chem. Phys. Lett. **357**, 85 (2002).

[18] T. Witte, T. Hornung, L. Windhorn, D. Proch, R. de Vivie-Riedle, M. Motzkus, and K. L. Kompa, Controlling molecular ground-state dissociation by optimizing vibrational ladder climbing, J. Chem. Phys. **118**, 2021 (2003).

[19] D. J. Maas, D. I. Duncan, A. F. G. van der Meer, W. J. van der Zande, and L. D. Noordam, Vibrational ladder climbing in NO by ultrashort infrared laser pulses, Chem. Phys. Lett. **270**, 45 (1997).

[20] L. Windhorn, J. S. Yeston, T. Witte, W. Fuß, M. Motzkus, D. Proch, K.-L. Kompa, and C. B. Moore, Getting ahead of IVR: A demonstration of mid-infrared induced molecular dissociation on a sub-statistical time scale, J. Chem. Phys. **119**, 641 (2003).

[21] C. Ventalon, J. M. Fraser, M. H. Vos, A. Alexandrou, J.-L. Martin, and M. Joffre, Coherent vibrational climbing in carboxyhemoglobin, Proc. Natl. Acad. Sci. USA **101**, 13216 (2004).

[22] M. Jewariya, M. Nagai, and K. Tanaka, Ladder climbing on the anharmonic intermolecular potential in an amino acid microcrystal via an intense monocycle terahertz pulse, Phys. Rev. Lett. **105**, 203003 (2010).

[23] S. Chelkowski, A. D. Bandrauk, and P. B. Corkum, Efficient molecular dissociation by a chirped ultrashort infrared laser pulse, Phys. Rev. Lett. **65**, 2355 (1990).

[24] D. B. Strasfeld, S.-H. Shim, and M. T. Zanni, Controlling vibrational excitation with shaped Mid-IR pulses, Phys. Rev. Lett. **99**, 038102 (2007).

[25] I. Morichika, K. Murata, A. Sakurai, K. Ishii, and S. Ashihara, Molecular ground-state dissociation in the condensed phase employing plasmonic field enhancement of chirped mid-infrared pulses, Nat. Commun. **10**, 3893 (2019).

[26] See Supplemental Material at http://link.aps.org/supplemental/10.1103/PhysRevResearch.6.L042058 for details about the measurement sample, the numerical simulation, determination of rotational constants and the description of 2D spectrum.

[27] D. Bailly, R. Farrenq, G. Guelachvili, and C. Rossetti, $^{12}C^{16}O_2$ analysis of emission fourier spectra in the 4.5-μm region:

Rovibrational transitions $0v_2^l v_3 - 0v_2^l(v_3 - 1)$, $v_2 = l$, J. Mol. Spectrosc. **90**, 74 (1981).

[28] I. Morichika, H. Tsusaka, and S. Ashihara, Generation of high-lying vibrational states in carbon dioxide through coherent ladder climbing, J. Phys. Chem. Lett., **15** 4662 (2024).

[29] K. C. Gronborg, S. M. Giles, and S. Garrett-Roe, Rotationally-resolved two-dimensional infrared spectroscopy of CO_2(g): Rotational wavepackets and angular momentum transfer, J. Phys. Chem. Lett. **13**, 8185 (2022).

[30] G. Kowzan and T. K. Allison, Theory of rotationally resolved two-dimensional infrared spectroscopy including polarization dependence and rotational coherence dynamics, Phys. Rev. A **106**, 042819 (2022).

[31] A. Mandal, G. Ng Pack, P. P. Shah, S. Erramilli, and L. D. Ziegler, Ultrafast two-dimensional infrared spectroscopy of a quasifree rotor: *J* scrambling and perfectly anticorrelated cross peaks, Phys. Rev. Lett. **120**, 103401 (2018).

[32] T. A. Wells, A. K. Muthike, J. E. Robinson, and P. C. Chen, High resolution coherent three dimensional spectroscopy of NO_2, J. Chem. Phys. **142**, 212426 (2015).

[33] A. Stolow and Y. T. Lee, Photodissociation dynamics of CO_2 at 157.6 nm by photofragment-translational spectroscopy, J. Chem. Phys. **98**, 2066 (1993).

[34] J. Quan, F. Muttaqien, T. Kondo, T. Kozarashi, T. Mogi, T. Imabayashi, Y. Hamamoto, K. Inagaki, I. Hamada, Y. Morikawa, and J. Nakamura, Vibration-driven reaction of CO_2 on Cu surfaces via Eley-Rideal-type mechanism, Nat. Chem. **11**, 722 (2019).

[35] N. Mukherjee and R. N. Zare, Preparation of polarized molecules using coherent infrared multicolor ladder excitation, J. Chem. Phys. **132**, 154302 (2010).

[36] W. E. Perreault, H. Zhou, N. Mukherjee, and R. N. Zare, Coherent preparation of highly vibrating and rotating D_2 molecules, J. Phys. Chem. Lett. **13**, 4682 (2022).

[37] M. Tsubouchi and T. Momose, Rovibrational wave-packet manipulation using shaped midinfrared femtosecond pulses toward quantum computation: Optimization of pulse shape by a genetic algorithm, Phys. Rev. A **77**, 052326 (2008).